論文 / 著書情報
Article / Book Information

論題(和文)	
Title	Study on Roller-Walker — Improvement of Locomotive Efficiency of Quadruped Robots by Passive Wheels
著者(和文)	遠藤 玄, 広瀬 茂男
Authors	Gen Endo, Shigeo Hirose
出典 / Citation	, Vol. 26, No. 8-9, pp. 969-988
Citation(English)	Advanced Robotics, Vol. 26, No. 8-9, pp. 969-988
発行日 / Pub. date	2012, 7
権利情報 / Copyright	本著作物の著作権は日本ロボット学会に帰属します。 Copyright (c) 2012 The Robotics Society of Japan.

Advanced Robotics

Publication details, including instructions for authors and subscription information:
http://www.tandfonline.com/loi/tadr20

Study on Roller-Walker — Improvement of Locomotive Efficiency of Quadruped Robots by Passive Wheels

Gen Endo [a] & Shigeo Hirose [a]

[a] Department of Mechanical and Aerospace Engineering, Tokyo Institute of Technology, I1-60, 2-12-1, Ookayama, Meguro-ku, Tokyo, 152-8552, Japan

Version of record first published: 24 Jul 2012

To cite this article: Gen Endo & Shigeo Hirose (2012): Study on Roller-Walker — Improvement of Locomotive Efficiency of Quadruped Robots by Passive Wheels, Advanced Robotics, 26:8-9, 969-988

To link to this article: http://dx.doi.org/10.1163/156855312X633066

VSP

Advanced Robotics 26 (2012) 969–988

ADVANCED ROBOTICS
brill.nl/ar

Full paper

Study on Roller-Walker — Improvement of Locomotive Efficiency of Quadruped Robots by Passive Wheels

Gen Endo * **and Shigeo Hirose**

Department of Mechanical and Aerospace Engineering, Tokyo Institute of Technology, I1-60, 2-12-1, Ookayama, Meguro-ku, Tokyo 152-8552, Japan

Received 3 June 2011; accepted 11 July 2011

Abstract

Roller-Walker is a leg–wheel hybrid mobile robot using a passive wheel equipped on the tip of each leg. The passive wheel can be transformed into sole mode by rotating the ankle roll joint when Roller-Walker walks on a rough terrain. This paper discusses the energy efficiency of locomotion in wheeled mode. We define a leg trajectory to produce forward straight propulsion, and discuss the relationships between the parameters of the leg trajectory and energy efficiency of the propulsion using a dynamics simulator. We find optimum parameter sets where optimization criterion is specific resistance. The results indicate that faster locomotion achieves higher energy efficiency. We then carry out hardware experiments and empirically derive the experimental specific resistance. We show that wheeled locomotion has an 8-times higher energy efficiency than the ordinary crawl gait. Finally, we compare the specific resistance of Roller-Walker with other walking robots described in the literature.

Keywords

Leg–wheel hybrid robot, Roller-Walker, roller skating, energy efficiency, specific resistance

1. Introduction

A walking robot that can select a discrete foot placement with an articulated leg has potential capabilities: (i) it can move adaptively on a rugged terrain, (ii) it has higher energy efficiency than a wheeled vehicle on soft deformable terrain because it leaves discrete footprints, whereas a wheeled vehicle makes a continuous furrow that requires a larger traction force, (iii) it makes holonomic and omnidirectional motion without slip, and (iv) it can be a stable and movable platform for a manipulator even on a rugged terrain when it is not walking. Many walking robots have

* To whom correspondence should be addressed. E-mail: gendo@mes.titech.ac.jp

 DOI:10.1163/156855312X633066

been developed to move on a rugged terrain so far and nowadays some robots edge closer to practical use [1, 2].

However, on a hard flat terrain, wheeled locomotion is absolutely better than legged locomotion in terms of moving velocity and energy efficiency. Therefore, many researchers have attempted to combine the advantages of these two types of locomotion through leg–wheel hybrid vehicles [3–6].

In these previous studies, most of the hybrid vehicles were equipped with driven wheels, which requires actuators to drive the wheels. Since driven wheels require control systems, and tend to be heavy and bulky, hybrid vehicles increase the complexity of the control systems and the total weight of the robot. In particular, increasing the weight of the robot due to hybridization restricts the walking performance because the walking vehicle is already heavy enough due to many degrees of freedom in the leg mechanisms.

Therefore, we have proposed a leg–wheel hybrid vehicle with passive wheels, which are the simplest and lightest wheels [7]. Passive wheels can minimize additional weight for hybridization and do not reduce the potential walking performance of the robot. Figure 1 shows an overview of the prototype robot of Roller-Walker. Roller-Walker is equipped with a passive wheel on the tip of each leg and the passive wheel can be transformed into sole mode by rotating the ankle roll joint when Roller-Walker walks on a rough terrain. Roller-Walker can utilize the legs' actuators and propel efficiently by means of the same principle as roller-skating on flat ground. This concept can be applied to other existing walking robots with a slight modification.

In our previous work, we named the wheeled locomotion as 'Roller-Walk' and derived the basic leg trajectories, such as straight, circular and rotational propulsion, where the evaluation criterion is the maximization of velocity [7]. We also proposed a leg trajectory adjustment method to track a specified velocity on the

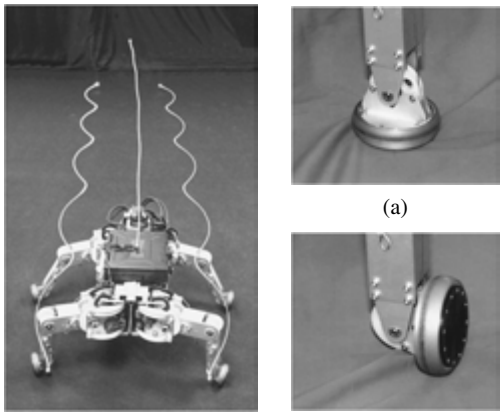

(a)

(b)

Figure 1. Roller-Walker. White lines show trajectories of the frontal leg ends and the body (left). Passive wheel in two modes (right). (a) Walking mode; (b) skating mode.

friction changing ground, and discuss the relationships between the leg trajectory and propulsive force/velocity characteristics in detail [8].

However, an improvement of locomotion efficiency by Roller-Walk remains a qualitative consideration and we have not yet discussed it. To the best of our knowledge, there is no detailed report addressing quantitative effectiveness of passive wheel locomotion in terms of energy efficiency in the previous studies, including biped robots with passive wheels [9, 10].

In this paper, we focus on the relation between the leg trajectory of Roller-Walk and energy efficiency of locomotion. We choose specific resistance [11] as an evaluation criterion and optimize the leg trajectory parameters by using a dynamics simulator. We then carry out hardware experiments to measure electrical power consumption and confirm that the results of the hardware experiments had a similar tendency to the dynamics simulations. Finally, we compare the efficiency of Roller-Walker with that of the crawl gait, which is a typical gait of a quadruped. We also show a comparison of Roller-Walker's specific resistance with other walking robots described in the literature.

2. Dynamics Simulator

In this paper, we choose specific resistance at steady state as an evaluation criterion, which is calculated by power consumption and propulsive velocity during locomotion, as we mention in the next section. In our previous work, we developed a simplified numerical simulator that only addressed the dynamics of the center of gravity of the robot, and addressed the frictional forces between the passive wheels and the ground [8]. Although the simplified single-point-mass simulator could derive the power consumed by the passive wheels, the simulator could not calculate any power that relates to the hardware configuration of the robot, such as mechanical joint power and electrical joint power. Therefore, we decided to develop a new dynamics simulator that has multi-joints and multi-links to form a concrete structure of the robot for a more detailed discussion.

2.1. Roller-Walker Modeling

We use a free open-source dynamics library, 'Open Dynamics Engine' (ODE), originally developed by Russell Smith [12]. Since the ODE is for computer games simulation, we investigated the ODE performance as a robotics research tool in terms of calculation speed and accuracy. In our previous work, we developed a quadruped robot simulator for 'TITAN-VIII' and verified that the simulated results nicely follow the experimental results with sufficient accuracy [13].

We model Roller-Walker based on the 'TITAN-VIII' simulator shown in Fig. 2. The rigid links are created by rectangular solids and cylinders, and they are connected by hinge joints. The size and mass of the link as well as joint positions are adopted from the design drawings and Refs [14, 15]. The total weight of the robot including batteries and control/measurement laptop PCs is 37.6 kg. We set the simulation time step as 1 ms and it takes 60 s to simulate 10 s of crawl gait.

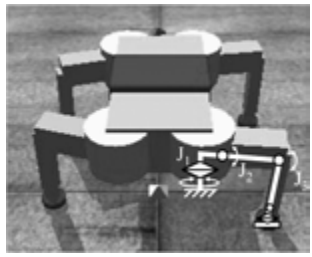

Figure 2. Screenshot of the Roller-Walker model in ODE.

2.2. Contact Model Setting

ODE automatically generates a virtual joint at the colliding point between the rigid bodies, and applies a force at the joint in order to simulate the collision and friction. In our preliminary experiments, we measured the frictional coefficients of the passive wheel on a vinyl floor sheet. We obtained $\mu_t = 0.0264$ and $\mu_n = 0.417$ in the tangential direction (rolling direction) and normal direction (axis direction), respectively. We carefully tuned the parameters, soft_erp and soft_cfm, which determine the stiffness of the ground in order not to diverge the numerical calculation. We introduce μ_n in the parameter mu to model the Coulomb frictional force in the normal direction of the passive wheel. We observed an unstable torque oscillation in the joint torque data when we only set the parameter for the friction pyramid approximation. Thus, in order to increase the numerical stability, we introduced a small force-dependent slip (dContactSlip1, 2) whose magnitude is 0.001.

```
dContact contact[10];
contact[i].surface.mode =
  dContactSlip1 | dContactSlip2 | dContactSoftERP |
  dContactSoftCFM | dContactApprox1;
contact[i].surface.mu       = 0.417;
contact[i].surface.slip1    = 0.001;
contact[i].surface.slip2    = 0.001;
contact[i].surface.soft_erp = 0.2;
contact[i].surface.soft_cfm = 0.0001;
```

We also introduce a rolling resistant torque τ_{wh} to the each passive wheel assuming Coulomb friction as:

$$\tau_{wh} = -\mathrm{sgn}(\omega_{wh})\mu_t F_z r_{wh}. \tag{1}$$

where sgn(∗) is the signum function, ω_{wh} is the angular velocity of the passive wheel and F_z is the vertical reaction force acting on the ground contact point. Both ω_{wh} and F_z are obtained by using ODE API(). $r_{wh} = 0.0425$ m is the radius of the passive wheel.

3. Specific Resistance

3.1. Definition of Specific Resistance

A dimensionless quantity specific resistance ε [11] is widely used to evaluate the efficiency of locomotion:

$$\varepsilon = \frac{E}{mg \cdot L}, \tag{2}$$

where E is the required energy for locomotion, m is the total mass of the vehicle, g is the gravity acceleration and L is the traveling distance. We can rewrite the above equation with a power consumption P and velocity V by differentiating both numerator and denominator as:

$$\varepsilon = \frac{\mathrm{d}E/\mathrm{d}t}{mg \cdot \mathrm{d}L/\mathrm{d}t} = \frac{P}{mg \cdot V}. \tag{3}$$

The smaller specific resistance indicates higher energy efficiency. For examples, specific resistance of a sliding object whose dynamic friction coefficient is μ becomes μ, indicating the smaller μ provides the higher efficiency of locomotion. This result agrees with our intuitive understanding.

However, when we look at (3), one question arises. What kind of power should we use? For example, should we use the pure mechanical power of the joint or the total electric power supplied by the battery? The derived specific resistance largely depends on the power used for calculation and each 'different level' of power provides us with important information. In this paper, we use three different powers to derive the specific resistance.

3.2. Specific Resistances Derived with Three Different Power Consumptions

The most fundamental and purest power consumption is the mechanical power consumption P_{wh} between the passive wheels and the ground. We define specific resistance $\varepsilon_{\mathrm{wh}}$ as:

$$\varepsilon_{\mathrm{wh}} = \frac{P_{\mathrm{wh}}}{mg \cdot V} = \frac{1}{mg \cdot V}\left(\sum^{i} \tau_{\mathrm{wh}}\omega_{\mathrm{wh}} + \sum^{i} F_{\mathrm{n}}V_{\mathrm{n}}\right), \tag{4}$$

where τ_{wh} and ω_{wh} are the rolling resistant torque and rolling velocity of the passive wheel, respectively, and F_{n} and V_{n} are the force and velocity of the passive wheel in the normal direction with respect to the ground. i indicates the number of wheels.

Secondly, specific resistance using the mechanical joint power consumption ε_{j} is obtained by:

$$\varepsilon_{\mathrm{j}} = \frac{P_{\mathrm{j}}}{mg \cdot V} = \frac{1}{mg \cdot V}\left(\sum^{k} \tau_{\mathrm{j}}\omega_{\mathrm{j}}\right), \tag{5}$$

where P_{j} is the mechanical joint power, k indicates the number of joints, and τ_{j} and ω_{j} are the joint torque and joint velocity obtained from ODE, respectively. Theoretically speaking, $\varepsilon_{\mathrm{wh}} = \varepsilon_{\mathrm{j}}$ because P_{j} equals P_{wh}. However, practically speaking,

a negative power generated by gravity cannot be fully stored and almost all negative power is dissipated as heat in the actuator. Therefore, the required mechanical joint power that is supplied by the actuator is redefined as:

$$\varepsilon_{\mathrm{j}} = \frac{P_{\mathrm{j}}}{mg \cdot V} = \frac{1}{mg \cdot V}\left(\sum^{k} [\tau_{\mathrm{j}}\omega_{\mathrm{j}}]^{+}\right), \tag{6}$$

where the function $[*]^{+}$ returns zero when the argument is a negative value.

Thirdly, since a DC servo actuator is installed on each joint, specific resistance with the electrical joint power consumption ε_{e} is obtained by:

$$\varepsilon_{\mathrm{e}} = \frac{P_{\mathrm{e}}}{mg \cdot V} = \frac{1}{mg \cdot V}\left(\sum^{k} V_{\mathrm{a}} i_{\mathrm{a}}\right), \tag{7}$$

where P_{e}, V_{a} and i_{a} are electric power, input voltage and input current to the actuator, respectively. See the Appendix for the actuator modeling.

3.3. Advantages and Drawbacks of $\varepsilon_{\mathrm{wh}}$, ε_{j} and ε_{e}

We define three specific resistances $\varepsilon_{\mathrm{wh}}$, ε_{j} and ε_{e} with different power consumptions. Here, we summarize the advantages and drawbacks of each of the indicators.

$\varepsilon_{\mathrm{wh}}$ is pure mechanical power consumption, and provides us with fundamental information about the relation of the wheel trajectory and energy efficiency regardless of the actual configuration of the robot. $\varepsilon_{\mathrm{wh}}$ expresses the possible maximum efficiency of the Roller-Walk, which is applicable to any kind of passive wheeled locomotion. However, it is very difficult to experimentally measure $\varepsilon_{\mathrm{wh}}$ with the hardware system because it requires precise measurements of the frictional force and slipping velocity of the passive wheels.

ε_{j} is derived from mechanical joint power and depends on the actual mechanism of the robot as well as the posture of the robot because the joint torque and velocity depend on the Jacobian matrix. Although we can discuss the optimum leg configuration and posture for a specific robot, it is difficult to experimentally measure ε_{j} because it requires velocity and torque sensors for each joint.

ε_{e} is calculated from electric power consumption in actuators. ε_{e} includes various hardware-related factors such as the efficiency of the actuator, the efficiency of the reduction gear system and the intractable friction of the joint driving system. Thus, it is impossible to generalize the result to another robot with a different leg configuration and/or different actuators. However, ε_{e} represents the total energy efficiency of a mobile vehicle, which is very important practical information. Moreover, electric power measurement is very easy to carry out and many previous works performed the measurement to evaluate robotic systems. Thus, we can discuss the relative performance of the locomotion by making a comparison between Roller-Walker and other walking robots.

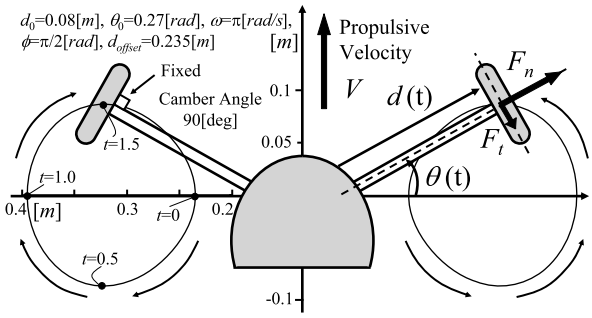

Figure 3. Kinematic model and an example of the leg trajectory (left).

4. Dynamics Simulation

4.1. Leg Trajectory

To simplify the problem, we assume that all legs are in the support phase, and the left and right legs move symmetric and periodic (Fig. 3). The leg trajectory is expressed as:

$$d(t) = d_{\text{offset}} + d_0(\sin(\omega t + 3\pi/2) + 1) \tag{8}$$

$$\theta(t) = -\theta_0 \sin(\omega t + 3\pi/2 + \phi), \tag{9}$$

where d_0 and θ_0 are amplitudes of sinusoidal oscillation in the normal and tangential directions of the passive wheel, respectively. ω determines the angular velocity of the leg trajectory oscillation. ϕ is the phase difference between the oscillations in the normal and tangential direction (here, we introduce appropriate offsets $(3\pi/2)$ considering the initial posture, the initial acceleration of the robot from zero velocity and the leg's workspace of the hardware prototype). There are four control parameters, d_0, θ_0, ω and ϕ, to modulate the leg trajectory in (8) and (9). An example of the leg trajectory is illustrated in Fig. 3.

When we assume Coulomb friction at a contact point of the passive wheel on the ground, the resulting tangential force $F_{\text{t}}(t)$ and normal force $F_{\text{n}}(t)$ due to the periodic leg motion can be expressed as:

$$F_{\text{t}}(t) = -\text{sgn}(V\cos\theta(t) + d(t)\dot{\theta}(t))\mu_{\text{t}}mg/4 \tag{10}$$

$$F_{\text{n}}(t) = -\text{sgn}(V\sin\theta(t) + \dot{d}(t))\mu_{\text{n}}mg/4, \tag{11}$$

where V is propulsive velocity. In reality, we designed a special passive wheel using a rigid aluminium disk wrapped with a molded thin hard urethane rubber in order to satisfy the assumption of the Coulomb friction model [14]. We also experimentally verified (10) and (11) using the hardware setup in our preliminary experiments. The same kinematic model is applied to the hind legs and we introduce a phase difference of $\phi_{\text{fr}} = 3\pi/2$ rad between the frontal and hind legs in order to minimize

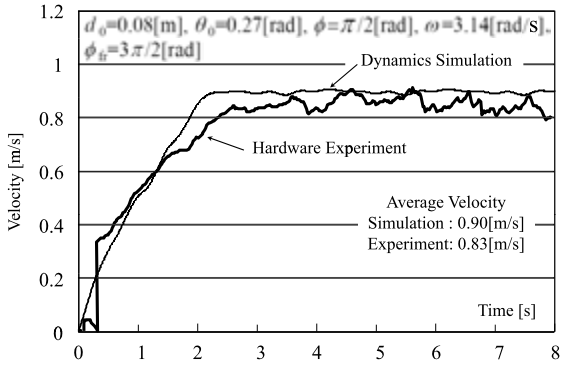

Figure 4. Example of a velocity simulation using the dynamics simulator.

the velocity fluctuation at steady state [7]. Since leg motions are symmetric, the lateral forces are canceled and the sagittal forces remain as a traction force.

We can derive a necessary condition of propulsion as:

$$|F_{\mathrm{n}}(t)\sin\theta(t)| > |F_{\mathrm{t}}(t)\cos\theta(t)|. \tag{12}$$

Here, by substituting (10) and (11) in (12), we obtain:

$$|\theta(t)| > \tan^{-1}(\mu_{\mathrm{t}}/\mu_{\mathrm{n}}). \tag{13}$$

Equation (13) indicates that $\theta(t)$ to perform propulsion should be larger than the minimum value, which is determined by a ratio of friction coefficients of the tangential and normal direction. The dynamics simulator developed in Section 2 does not strictly satisfy (13) because force-dependent slip, which generates slipping velocity proportional to the applied tangential force, is introduced to increase the numerical stability of the dynamics calculation. However, the fundamental characteristics of wheeled propulsion are not so different from the Coulomb friction model because the force-dependent slip parameter is set to a very small value.

We show a typical example of velocity simulation with a hardware experiment in Fig. 4. Simulated velocity is close to the measured actual velocity with an accuracy of 8.4% error when it reaches the steady velocity.

4.2. Optimization of the Leg Trajectory

In this section, we derive an optimum leg trajectory using the dynamics simulator for a straight steady propulsion that minimizes specific resistance.

Here, we have four control parameters (d_0, θ_0, ω, ϕ) to modulate the leg trajectory. In our previous work, we studied the optimum parameters to achieve maximum propulsive velocity of the robot at steady state [7]. We found that the generated velocity V is proportional to ω and $\phi = \pi/2$ is desirable. As for ω, the result is reasonable because (10) and (11) do not depend on the magnitude of V and thus the larger ω supplies the larger propulsive power proportional to ω. Therefore, ω does not affect the mechanical specific resistance $\varepsilon_{\mathrm{wh}}$ and ε_{j}. As for ϕ, we can analytically derive a geometrical constraint $\phi = \pi/2$, where the passive wheel does not

generate the velocity in the normal direction assuming that V is constant and $\theta(t)$ is prescribed by a sine wave. Thus, in the following discussion we set $\omega = \pi$, $\phi = \pi/2$ and focus on (d_0, θ_0) — the amplitudes of the oscillation in the normal direction and tangential direction. In the case of our experimental setup, the maximum values of d_0 and θ_0 within the leg's workspace are 0.08 m and 0.4 rad, respectively.

Figure 5 shows specific resistance $\varepsilon_{\mathrm{wh}}$ derived from the mechanical power consumption between the passive wheels and the ground. $\varepsilon_{\mathrm{wh}}$ keeps almost constant in the range of $0.12 \leqslant \theta_0 \leqslant 0.4$ and the larger d_0 slightly improves $\varepsilon_{\mathrm{wh}}$. $\varepsilon_{\mathrm{wh}}$ extremely increases where $\theta_0 < 0.11$ because the robot rapidly decreases the propulsive velocity due to a violation of the necessary condition of (13). The minimum $\varepsilon_{\mathrm{wh}} = 0.0361$ is achieved where $d_0 = 0.08$ m and $\theta_0 = 0.2$ rad. The vertical axis on the right in Fig. 5 indicates a ratio of specific resistance $\varepsilon_{\mathrm{wh}}$ and the tangential friction coefficient μ_{t}. The averaged value of the ratio $\varepsilon/\mu_{\mathrm{t}}$ is 1.4 where $0.11 \leqslant \theta_0 \leqslant 0.4$ and $d_0 = 0.08$ m. This result suggests that the leg trajectory with these parameters hardly generates a slipping loss in the normal direction and the required power is mainly consumed by a rolling resistance in the tangential direction. Therefore, we can consider the leg trajectory described by the simple sinusoidal equations (8) and (9) is sufficient to generate energy-efficient wheeled locomotion.

Figure 6 shows specific resistance ε_{j} derived from the mechanical power consumption of the joints. The smaller θ_0 but larger than 0.12 permits the robot to propel with smaller ε_{j}. However, as for d_0, the smaller $d_0 = 0.03$ has a higher en-

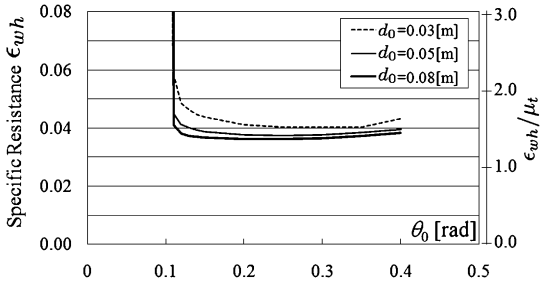

Figure 5. Specific resistance $\varepsilon_{\mathrm{wh}}$ with respect to (d_0, θ_0).

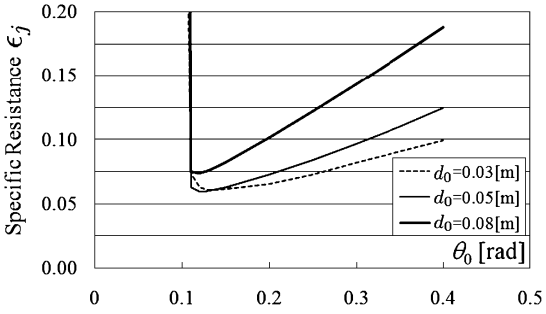

Figure 6. Specific resistance ε_{j} with respect to (d_0, θ_0).

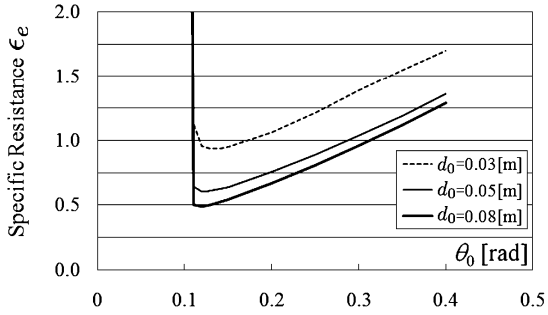

Figure 7. Specific resistance ε_e with respect to (d_0, θ_0).

ergy efficiency than $d_0 = 0.08$. This result suggests that the larger d_0 generates more negative power. The magnitude of ε_j is about 1.3–4.9 times larger than ε_{wh}. Thus, we consider an energy effective leg configuration and posture of the robot are more important than only focusing on the relative trajectory of the passive wheel with respect to the ground.

Figure 7 shows specific resistance ε_e derived from the electric power consumption with a DC actuator model. The most distinct result is that the magnitude of ε_e is about 20-times larger than ε_{wh}, suggesting that the actual hardware implementation is really dominant and practically very important to improve the overall energy efficiency. The smaller θ_0 but larger than 0.12 produces the smaller ε_e and the larger d_0 also achieves the smaller ε_e. The optimum parameters for the minimum $\varepsilon_e = 0.488$ are $d_0 = 0.08$ m and $\theta_0 = 0.12$ rad, which are almost the same parameters for the maximum velocity. The result indicates that the higher velocity achieves more energy-efficient locomotion.

5. Hardware Experiment

In the previous section, the required mechanical power with the optimized trajectory is almost the same power for the rolling resistance of the passive wheels. However, it is difficult to accurately measure the tangential frictional force because the absolute value is very small. On the other hand, the total electric power measurement is very easy and beneficial to improve the actual hardware system. Therefore, we measure specific resistance ε_e experimentally by measuring the electric power.

5.1. Measurement Method

We measured the battery current by using a current sensor (NEC/TOKIN MDCS) and also measured the battery voltage. At the beginning of the experiment, we measured the electric power consumption as 'basal metabolism' where Roller-Walker took a standard posture and the main body was supported by a stand in order to lift up all legs from the ground. To derive net specific resistance, we assumed this basal metabolism power is constant and subtracted the power from the measured total

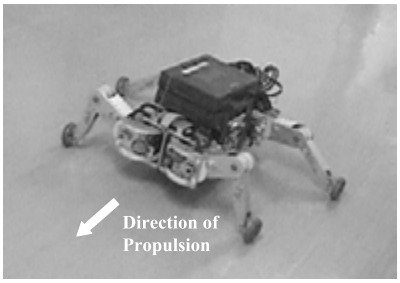

Figure 8. Measurement of experimental specific resistance (lowering body height provides the larger d_0).

electric power of locomotion experiments. We confirmed that the basal metabolism power is 82.0 W, which is mainly consumed by 12 servo driver circuits.

We also measured the velocity using a tachogenerator attached to an additional passive wheel for dead reckoning under the main body. Figure 8 shows a snapshot of the measurement experiment on the vinyl floor. All measurement devices and a control computer were mounted on the main body. We set a low body height in order to maximize d_0. To generate smooth acceleration from zero velocity at the beginning of each experiment, we set the lower ω and the higher θ_0, and gradually changed them to the target parameter set by a manual operation. Additionally, we also added a steering offset to $\theta(t)$ because the direction of propulsion was changed due to the slight undulation of the experimental floor. The manual adjustment was terminated when a steady straight propulsion was established, which typically took 50 m traveling distance. We did obtained two measurements for each parameter set and averaged the results.

5.2. Specific Resistance ε_e in Roller-Walker

To verify the relation between the leg trajectory parameters and specific resistance, we performed parametric measurements. The results are shown with numerical simulations.

First, we discuss ω, which determines the angular velocity of the leg trajectory. As we expected, Fig. 9a indicates that the larger ω produces a larger velocity and power consumption, although net specific resistance remains relatively constant. Thus, this result supports our physical understanding mentioned in Section 4.2, namely, that ω does not affect the specific resistance. Moreover, this result also suggests that a propulsive velocity control adjusting ω can be achieved without affecting the efficiency of locomotion. This is a nice and useful characteristic because once we find an energy-efficient optimum leg trajectory, we can keep the maximum efficiency regardless of the propulsive velocity.

Figure 9b shows the result of dynamics simulation with the same leg trajectory parameters. The propulsive velocity and power are proportional to ω, which is similar to the experimental result. However, the gradient of the simulated power consumption is smaller than the experimental power consumption, which produces

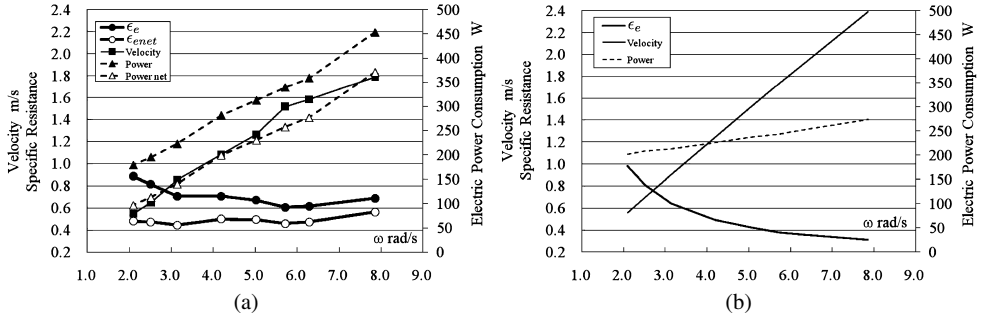

Figure 9. Relation between ω and experimental specific resistance, velocity and power: $d_0 = 0.05$ m, $\theta_0 = 0.15$ rad, $\phi = \pi/2$ rad and $\phi_{\mathrm{fr}} = 3\pi/2$ rad. (a) Hardware experiment; (b) dynamics simulation.

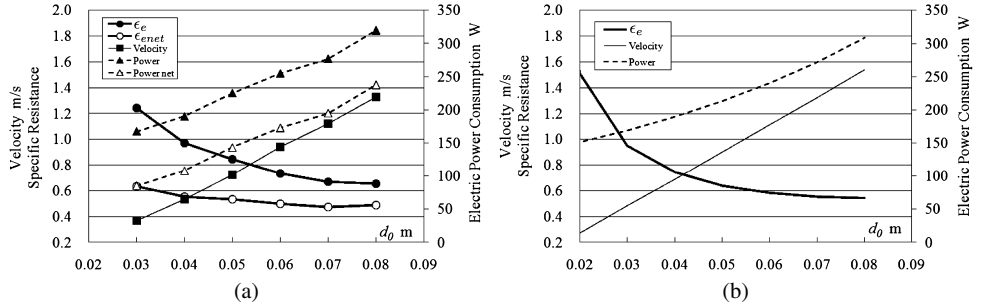

Figure 10. Relation between d_0 and experimental specific resistance velocity and power: $\theta_0 = 0.15$ rad, $\omega = 3.14$ rad/s, $\phi = \pi/2$ rad and $\phi_{\mathrm{fr}} = 3\pi/2$ rad. (a) Hardware experiment; (b) dynamics simulation.

smaller ε_{e} with larger ω. The reason would be a contact modeling error of the passive wheel in the larger ω and/or a current-related energy loss in the actuation system in the hardware.

Secondly, we discuss d_0, the amplitude of the nominal oscillation, which also relates to the propulsive energy input. Figure 10a shows that the larger d_0 achieves larger velocity and power, and specific resistance slightly decreases with the larger d_0. The result of the dynamics simulation indicates a similar tendency shown in Fig. 10b. Thus, we define the maximum $d_0 = 0.08$ m within the leg's workspace as the optimum value of d_0.

Thirdly, we discuss θ_0, the amplitude of the tangential oscillation. In Fig. 11a, we could not carry out the measurement where $\theta_0 < 0.13$ rad because Roller-Walker could not propel and the required joint torques hit the current limitations of the electric system of the robot (thus, it is expected that hardware specific resistance would rapidly increase where $\theta_0 < 0.13$). Measured specific resistance shows a similar tendency to the dynamics simulation in Fig. 11b. The smaller θ_0 decreases specific resistance and the experimental value becomes a minimum at $\theta_0 = 0.15$ rad where the velocity is also maximized.

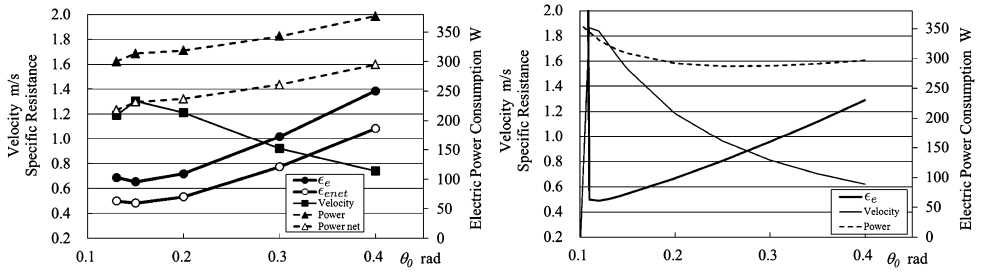

Figure 11. Relationship between θ_0 and experimental specific resistance velocity and power: $d_0 = 0.08$ m, $\omega = 3.14$ rad/s, $\phi = \pi/2$ rad and $\phi_{\mathrm{fr}} = 3\pi/2$ rad. (a) Hardware experiment; (b) dynamics simulation.

Finally, we empirically derived the optimum parameter set that minimizes specific resistance using this hardware prototype model. We obtained minimum specific resistance ε_{e} of 0.44 where $d_0 = 0.08$ m, $\theta_0 = 0.15$ rad, $\omega = 6.28$ rad/s, $\phi = \pi/2$ and $\phi_{\mathrm{fr}} = 3\pi/2$. The minimum specific resistance achieved is very close to the result of the dynamics simulation ($\varepsilon_{\mathrm{e}} = 0.488$). The total power required was 452 W and the velocity achieved was 2.27 m/s, which is about 11-times faster than the walking velocity.

5.3. Specific Resistance in the Crawl Gait

We measured the specific resistance in the crawl gait, which is the most typical static walking of quadrupeds. The standard walking posture was selected as in Ref. [15], and the step length and height are 0.18 and 0.05 m, respectively. We used a fixed duty factor of 0.75 and modulated the walking period to control the walking velocity from 0.01 to 0.12 m/s. When the walking velocity is larger than 0.04 m/s, we verified that net specific resistance is almost constant at 3.53, which is about 8 times higher than that of Roller-Walk. This result suggests that Roller-Walk remarkably improves the energy efficiency of locomotion on level ground. More detailed data is shown in Fig. 12.

6. Comparison with Other Walking Robots

It is very interesting and attractive to compare the specific resistance of the walking robots developed so far. However, it is sometimes misleading because one robot may have been developed to achieve high energy efficiency on well-prepared ground and another robot may have been developed to achieve a special mission negotiating over a rough terrain. Moreover, technically speaking, the derivation of power consumption is very controversial. One robot may use pure mechanical power of an actuator shaft and another may use total electric power supplied to the robot system, which includes many devices independent of locomotion itself. Nevertheless, it seems to be still beneficial to compare the specific resistance to understand the basic performance in terms of energy efficiency.

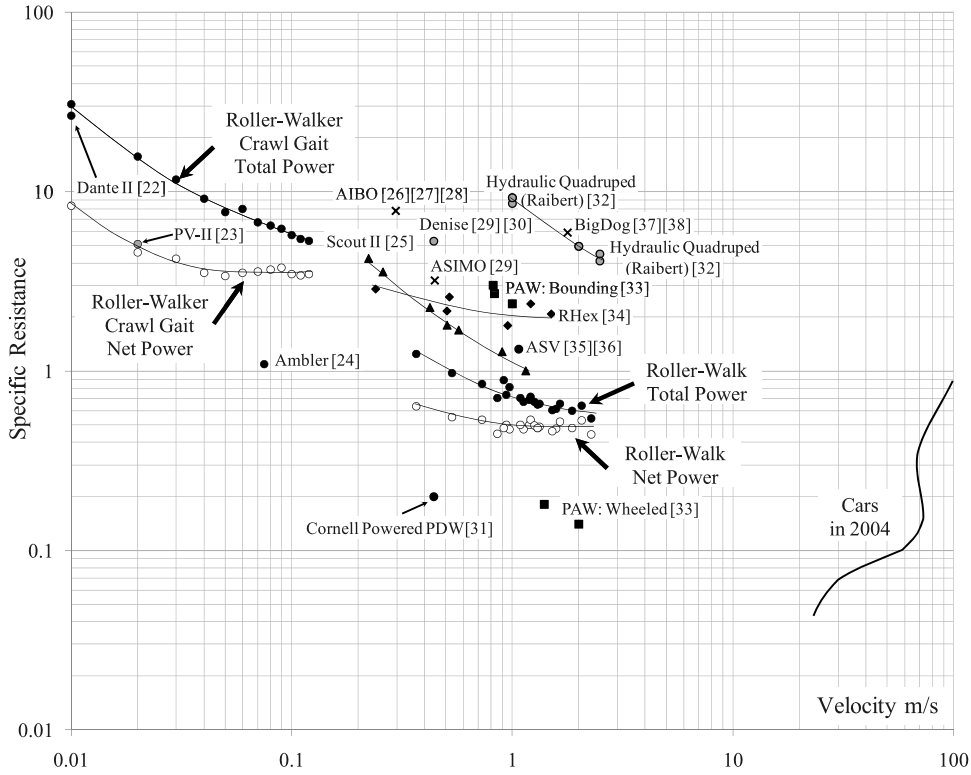

Figure 12. Velocity *versus* specific resistance of walking robots [22–38].

We calculated specific resistance with respect to velocity in Fig. 12. The robots in the right-bottom possess locomotion high performance. This diagram was originally proposed by Gabrielli and von Karman [11], and several researchers have updated the diagram from the viewpoint of robotics research (e.g., Refs [17, 18]). However, several data mentioned in Refs [17, 18] remain unclear how to derive their specific resistance and some references are very difficult to obtain at present. Therefore, we dare not directly refer to data in Refs [17, 18], but refer to the original references listed in Refs [17, 18]. Reference [19] also provides us with useful references to reach the original papers. Additionally, we also investigated the old but easily available online literature, such as technical reports open to the public, as well as the new walking robots in the last decade.

We focus on specific resistance with the electric power consumption ε_e. Thus, we do not plot specific resistance derived by the pure mechanical power such as McGeer's Passive Dynamic Walker [20]. The gray dots are calculated from the measured power supplied to the actuators while the black dots use the measured power supplied to the robot system from an energy source. The polygon black dots are also calculated from the battery power to the robot system and these robots use

a similar platform with a springy leg. The cross dots are estimated from the duration of batteries or maximum power output of an equipped engine.

Figure 12 clearly indicates that Roller-Walk improves the locomotion performance compared with the crawl gait. Roller-Walk is more energy efficient than any other rapid walker with a springy leg except for PAW in wheeled mode and the powered passive dynamic walker developed in Cornell university, which is a special elaborated biped to achieve extremely high energy efficiency (ARL Monopod I and II are not plotted in Fig. 12 because they are two-dimensional hoppers requiring special stabilizing facilities). Moreover, there is a possibility to increase the energy efficiency of the conventional robots by using the Roller-Walker concept because it only requires a slight mechanical modification.

One might think that Roller-Walk is better than usual wheeled locomotion. As a comparison, we show a black line indicating cars in 2004 adapted from Ref. [21]. Roller-Walk does not stand a chance of competing with cars because a legged robot usually requires many degrees of freedom with many servo drive systems that suffer from low energy efficiency. Thus, if a target environment is a completely smooth terrain, a conventional wheeled robot with a driven wheel is absolutely better than Roller-Walk. This argument is also supported by the high energy efficiency of PAW in wheeled mode. PAW is a quadruped robot that has a 1-d.o.f. springy leg and an active wheel at the tip of the leg. Thanks to the reduced degrees of freedom of the leg mechanism, PAW can achieve a higher energy efficiency than Roller-Walker in wheeled mode. However, the walking capability of PAW is very limited because PAW is specially designed for a bounding gait on a flat rigid terrain.

We believe that Roller-Walk provides a walking robot, which was originally developed to negotiate a rugged terrain, with a practical solution to increase locomotion efficiency on flat ground.

7. Conclusions

In this paper, we focus on the relation between the leg trajectory of Roller-Walk and energy efficiency of locomotion. We investigate the specific resistance of Roller-Walker using both dynamics simulations and hardware experiments. We confirmed that Roller-Walk improves the locomotion efficiency 8 times higher than the crawl gait. We compare the results with other walking robots, suggesting that Roller-Walk can be an effective solution to increase the efficiency of a walking robot on level ground.

In this paper, we measured specific resistance on a vinyl floor in an indoor environment. The specific resistance of Roller-Walk largely depends on the frictional coefficient in the tangential direction. Thus, there is a case that walking has higher energy efficiency than that of Roller-Walk when the tangential friction is very large, such as walking on sand. Automatic mode selection using energy efficiency from wheel to sole and vice versa forms one of our interesting future research topics.

Acknowledgements

The authors would like to thank Professor Edwardo Fumihiko Fukushima of Tokyo institute of Technology and Professor Keisuke Arikawa of Kanagawa Institute of Technology for the derivation of the electric power using the DC actuator model.

References

1. T. Doi, R. Hodoshima, Y. Fukuda, S. Hirose, J. Mori and T. Okamoto, Development of a quadruped walking robot to work on steep slopes, TITAN XI (walking motion with compensation for compliance), in: *Proc. Int. Conf. on Intelligent Robots and Systems*, Edmonton, AB, pp. 3413–3418 (2005).
2. F. Hardarson, Locomotion for difficult terrain, *Technical Report TRITA-MMK 1998:3*, Royal Institute of Technology, Stockholm (1998).
3. Y. Dai, E. Nakano, T. Takahashi and H. Ookubo, Motion control of leg–wheel robot for an unexplored rough terrain environment, in: *Proc. 7th Int. Conf. on Advanced Robotics*, Sant Feliu de Guixols, Vol. 2, pp. 911–916 (1995).
4. H. Adachi, N. Koyachi, T. Arai, A. Shimizu and Y. Nogami, Mechanism and control of a leg–wheel hybrid mobile robot, in: *Proc. Int. Conf. on Intelligent Robots and Systems*, Kyongju, pp. 1792–1797 (1999).
5. S. J. Ylonen and A. J. Halme, WorkPartner — centaur like service robot, in: *Proc. Int. Conf. on Intelligent Robots and Systems*, Lausanne, pp. 727–732 (2002).
6. Ch. Grand, F. BenAmar, F. Plumet and Ph. Bidaud, Decoupled control of posture and trajectory of the hybrid wheel-legged robot Hylos, in: *Proc. Int. Conf. on Robotics and Automation*, New Orleans, LA, pp. 5111–5116 (2004).
7. G. Endo and S. Hirose, Study on Roller-Walker (multi-mode steering control and self-contained locomotion), in: *Proc. Int. Conf. on Robotics and Automation*, San Francisco, CA, pp. 2808–2817 (2000).
8. G. Endo and S. Hirose, Study on Roller-Walker — adaptation of characteristics of the propulsion by a leg trajectory, in: *Proc. Int. Conf. on Intelligent Robots and Systems*, Nice, pp. 1532–1537 (2008).
9. M. Kumagai and K. Tamada, Wheel locomotion of a biped robot using passive rollers biped robot roller walking using a variable-curvature truck, *J. Robotics Mechatron.* **20**, 206–212 (2008).
10. K. Hashimoto, Y. Sugahara, H. Lim and A. Takanishi, Swizzle movement for biped walking robot having passive wheels, *J. Robotics Mechatron.* **20**, 413–419 (2008).
11. G. Gabrielli and T. H. von Karman, What price speed?, *Mech. Eng.* **72**, 775–781 (1950).
12. Open Dynamics Engine, http://www.ode.org/.
13. G. Endo, K. Arikawa and S. Hirose, Quantitative evaluations of torque/power simulations using a free dynamics simulator 'Open Dynamics Engine' — Comparison with TITAN-VIII hardware measurements, in: *Proc. Int. Conf. on Robotics and Automation*, Shanghai, pp. 6065–6070 (2011).
14. G. Endo and S. Hirose, Study on Roller-Walker (system integration and basic experiments), in: *Proc. Int. Conf. on Robotics and Automation*, Detroit, MI, pp. 2032–2037 (1999).
15. K. Arikawa and S. Hirose, Development of quadruped walking robot TITAN-VIII, in: *Proc. Int. Conf. on Intelligent Robots and Systems*, Osaka, pp. 208–214 (1996).
16. S. Hirose, *Robotics*, Shokabo Publishing, Tokyo (1987) (in Japanese).
17. P. Gregorio, M. Ahmadi and M. Buehler, Design, control, and energetics of an electrically actuated legged robot, *IEEE Trans. Syst. Man Cybernet. B* **27**, 626–634 (1997).

18. K. Dowling, Limbless locomotion: learning to crawl with a snake robot, *Technical Report CMU-RI-TR-97-48*, Robotics Institute, Carnegie Mellon University (1997).
19. D. Wettergreen, Robotic walking on natural terrain: gait planning and behavior-based control for statically-stable walking robots, *Technical Report CMU-RI-TR-95-42*, Robotics Institute, Carnegie Mellon University, Pittsburgh, PA (1995).
20. T. McGeer, Passive dynamic walking, *Int. J. Robotics Res.* **9**, 62–82 (1990).
21. J. Yong, R. Smith, L. Hatano and S. Hillmansen, What price speed — revisited, *INGENIA* **22**, 46–51 (2005).
22. J. E. Bares and D. S. Wettergreen, Technical description, results, and lessons learned, *Int. J. Robotics Res.* **18**, 621–649 (1999).
23. S. Hirose and Y. Umetani, The basic motion regulation system for a quadruped walking machine, in: *Proc. ASME Design Engineering Technical Conf.*, Beverly Hills, CA, pp. 1–6 (1980).
24. E. Krotkov and R. Simmons, Performance of a six-legged planetary rover: power, positioning, and autonomous walking, in: *Proc. Int. Conf. on Robotics and Automation*, Nice, pp. 169–174 (1992).
25. S. Talebi, I. Poulakakis, E. Papadopoulos and M. Buehler, Quadruped robot running with a bounding gait, in: *Proc. 7th Int. Symp. on Experimental Robotics*, Honolulu, HI (2000).
26. S. Chernova and M. Veloso, An evolutionary approach to gait learning for four-legged robots, in: *Proc. Int. Conf. on Intelligent Robots and Systems*, Sendai, pp. 2562–2567 (2004).
27. M. S. Kim and W. Uther, Automatic gait optimisation for quadruped robot, presented at: *Australian Conf. on Robotics and Automation*, Brisbane, QLD (2003).
28. http://esupport.sony.com/US/perl/model-documents.pl?mdl=ERA201B1.
29. S. Collins, A. Ruina, R. Tedrake and M. Wisse, Efficient bipedal robots based on passive-dynamic walkers, *Science* **307**, 1082–1085 (2005).
30. M. Wisse, Three additions to passive dynamic walking; actuation, an upper body, and 3D stability, in: *Proc. Int. Conf. on Humanoid Robots*, Santa Monica, CA, pp. 113–132 (2004).
31. S. Collins and A. Ruina, A bipedal walking robot with efficient and human-like gait, in: *Proc. Int. Conf. on Robotics and Automation*, Barcelona, pp. 1995–2000 (2005).
32. M. Raibert, H. B. Brown, M. Chepponis, J. Koechling, J. K. Hodgins, D. Dustman, W. K. Brennan, D. S. Barrett, C. M. Thompson, J. D. Hebert, W. Lee and L. Borvansky, Dynamically stable legged locomotion, *Technical Report 1179, LL-6*, Massachusetts Institute of Technology, Cambridge, MA (1989).
33. J. A. Smith, I. Poulakakis, M. Trentini and I. Sharf, Bounding with active wheels and liftoff angle velocity adjustment, *Int. J. Robotics Res.* **29**, 414–427 (2009).
34. D. Campbell and M. Buehler, Preliminary bounding experiments in a dynamic hexapod, *Exp. Robotics* **VIII**, 612–621 (2003).
35. D. R. Pugh, E. A. Ribble, V. J. Vohnout, T. E. Bihari, T. M. Walliser, M. R. Patterson and K. J. Waldron, Technical description of the adaptive suspension vehicle, *Int. J. Robotics Res.* **9**, 24–42 (1990).
36. K. J. Waldron and R. B. McGhee, The adaptive suspension vehicle, *IEEE Control Syst. Mag.* **6**(6), 7–12 (1986).
37. BostonDynamics, BigDog: the most advanced rough-terrain robot on Earth, http://www.bostondynamics.com/robot_bigdog.html.
38. BigDog Overview, http://www.bostondynamics.com/img/BigDog_Overview.pdf.
39. S. Hirose, Y. Uchida and R. Chu, Consideration of new tendon-driven mechanisms, in: *Proc. JSME Conf. on Robotics and Mechatronics*, Sendai, p. 1CI2-3 (1998) (in Japanese).

Appendix: Actuator Model

We assume that a DC motor can be expressed as an equivalent electric circuit shown in Fig. A.1 [16]. Table A.1 explains symbols representing physical quantities. It is generally known that a DC motor loses energy during energy conversion from electric energy to mechanical energy. These losses are known as copper loss, hysteresis loss, mechanical friction loss, etc. We model copper loss and other losses by introducing R_a and R_h in Fig. A.1. R_a is obtained by a direct measurement of armature electric resistance and R_h is estimated by the maximum efficiency of the motor and R_a. The maximum efficiency of the motor η_max, which is usually found in the data sheet, is expressed as $\eta_\mathrm{max} = (R_\mathrm{a}/R_\mathrm{h})(\sqrt{1 + R_\mathrm{h}/R_\mathrm{a}} - 1)^2$. We obtain R_h by solving this equation for R_h as $R_\mathrm{h} = 4\eta_\mathrm{max} R_\mathrm{a}/(1 - \eta_\mathrm{max})^2$.

The motor shaft torque τ_m and velocity ω_m without the reduction mechanism are calculated by using the joint torque τ_j and velocity ω_j obtained from ODE:

$$\tau_\mathrm{m} = \frac{\tau_\mathrm{j}}{\eta_\mathrm{g}\xi_\mathrm{g}} \tag{A.1}$$

$$\omega_\mathrm{m} = \xi_\mathrm{g}\omega_\mathrm{j}, \tag{A.2}$$

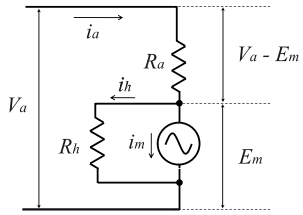

Figure A.1. Equivalent electric circuit of a DC motor.

Table A.1.
Definition of the symbols

Physical quantity	Symbol	Value	Unit
Input voltage to the actuator	V_a	—	V
Input current to the actuator	i_a	—	A
Voltage due to electormotive force	E_m	—	V
Armature resistance	R_a	2.27	Ω
Representing resistance for various loss	R_h	55.8	Ω
Torque constant	K	0.0118	Nm/A
Current to the ideal motor	i_m	—	A
Current to the R_h	i_h	—	A
Output torque of the motor	τ_m	—	Nm
Output velocity of the motor	ω_m	—	rad/s
Reduction ratio	ξ_g	693, 863, 551	—
Efficiency of the reduction mechanism	η_g	50	%

where η_g and ξ_g are efficiency and ratio of the velocity reduction mechanism, respectively. The actual velocity reduction mechanism is composed of a three-stage planetary gearhead and a wire–pulley mechanism. We estimate $\eta_g = 50\%$ because the efficiency of a single-stage planetary gear is 84% according to a similar gearhead (MAXON: GP26B) and the efficiency of the wire driving mechanism is estimated as 85% based on our previous measurement [39]. In the following calculation, we assume constant η_g regardless of the rotating velocity to simplify the analysis. The inherent characteristic of a DC motor satisfies the following:

$$E_m = K\omega_m \tag{A.3}$$

$$\tau_m = Ki_m. \tag{A.4}$$

The net current for the motor rotation i_m is expressed as:

$$i_m = \frac{V_a - E_m}{R_a} - \frac{E_m}{R_h}. \tag{A.5}$$

We obtain the input voltage to the actuator V_a by substituting (A.3) and (A.4) into (A.5):

$$V_a = R_a\left\{\frac{\tau_m}{K} + \left(\frac{1}{R_a} + \frac{1}{R_h}\right)K\omega_m\right\}. \tag{A.6}$$

The input current to the actuator i_a satisfies:

$$i_a = \frac{V_a - E_m}{R_a}. \tag{A.7}$$

By substituting (A.3) and (A.6) into (A.7), we obtain:

$$i_a = \frac{\tau_m}{K} + \frac{K\omega_m}{R_h}. \tag{A.8}$$

Finally, we can calculate ε_e in (7) by using V_a and i_a because τ_m and ω_m are estimated by (A.1) and (A.2) using ODE, and R_a, R_h and K are known constant parameters from the data sheet of the motor (Nippou Denki; MM26E).

About the Authors

Gen Endo received his BS, MS and PhD degrees from Tokyo Institute of Technology, Japan, in 1996, 1998 and 2000, respectively. From 2000 to 2007, he joined Sony Corp. and worked in the Advanced Telecommunication Research Institute, International as a Visiting Researcher. He joined the Faculty of Tokyo Institute of Technology, in 2007, where he is currently an Assistant Professor of the Department of Mechano-Aerospace Engineering.

Shigeo Hirose received his Doctoral Degree in Control Engineering from Tokyo Institute of Technology, in 1976. He is a Fellow of the IEEE. His research interests include the design and control of snake-like robots, walking robots, wheel and crawler vehicles, omnidirectional robots, wall-climbing robots, planetary exploration robots, and devices for the control of robots. He received the Pioneer in Robotics and Automation Award from the IEEE Robotics and Automation Society, in 1999, and Medal with Purple Ribbon from the Japanese Government, in 2006.